# Surface Quality Analysis of AZ31B Mg Alloy Sheet in Ultrasonic-Assisted Warm Single-Point Incremental Forming

**Juan Liao**
Fuzhou University
**Xiangshou Zeng**
Fuzhou University
**Xin Xue** ( xin@fzu.edu.cn )
Fuzhou University https://orcid.org/0000-0001-8021-6685

**Research Article**

**Keywords:** Single point incremental forming, Warm temperature, Ultrasonic vibration, Orange peel, Surface quality

**Posted Date:** August 5th, 2021

**DOI:** https://doi.org/10.21203/rs.3.rs-759067/v1



**Version of Record:** A version of this preprint was published at The International Journal of Advanced Manufacturing Technology on September 17th, 2021. See the published version at https://doi.org/10.1007/s00170-021-08045-8.

# Abstract

With a view to improving the surface quality of the magnesium (Mg) alloy at a warm temperature, the ultrasonic-assisted warm single point incremental forming (SPIF) is proposed. The surface quality of the Mg alloy during the warm SPIF is primarily affected by two parts: the orange peel patterns of the non-contact surface and the scratches and adhesive wear of the contact surface. In this work, the surface quality of the AZ31B Mg alloy sheet parts at different forming temperatures and ultrasonic amplitudes is evaluated by examining the surface roughness and topography. The results show that the generation of orange peel patterns is significantly affected by temperature. In addition, scratches and adhesive wear of the contact surface increase with the rising temperature. After applying the ultrasonic vibration (UV), the quality of both the non-contact and the contact surfaces of the parts are significantly improved, but too large ultrasonic amplitude slightly reduces the surface quality. Moreover, the microstructural examination results show that UV has a great effect on dynamic recrystallization and grain refinement, which positively affects surface quality improvement.


# 1. Introduction

Mg alloy enjoys the advantages of high specific strength and stiffness, good machinability, good shock absorption, high thermal conductivity, etc. It is popularly used in national defense, aerospace, chemical industry, automotive, biomedical, electronics, and other fields [1, 2]. Because of its crystal structure, Mg alloy has low formability and forming limit at room temperature and usually works in “warm conditions” [3, 4]. The warm Single Point Incremental Forming (SPIF) process is a highly flexible technology that can remarkably improve the formability and forming limit of Mg alloys [5, 6]. However, the orange peel patterns are sometimes observed on the non-contact surfaces of formed parts of Mg alloy in the warm SPIF. Strong abrasive and adhesive wear are also seen on the contact surfaces (which contact with the tool). They seriously affect the surface quality of the formed parts.

Recently, researchers have shown interest in the orange peel of non-contact surfaces in the warm SPIF process for Mg alloy. Leonhardt et al. [7] reported a conspicuous orange peel on the surface of the formed parts through the warm SPIF experiment using hot air. Varying degrees of roughening of orange peel on the surface appeared at different temperatures. Liao et al. [8] evaluated the influence of the heating modes on the orange peel phenomenon and suggested that the occurrence of orange peel patterns was significantly affected by the temperature distribution. Davis [9] and Carter et al. [10] reported that oversized grains were more likely to cause orange peel on the surface of the part. Antonyswamy et al. [11] believed that the appropriate temperature and rapid strain rate play a vital role in the orange peel effect. However, several researchers have focused on the wear of contact surfaces in the warm SPIF process. Duflou et al. [12] noticed that the increase in temperature significantly increased the contact friction coefficient of the parts, thereby affecting the surface quality of the contact surface. Xu et al. [13] investigated the causes of rough surface finish and concluded that the high temperature and contact pressure at the tool-sheet interface could cause scratches, resulting in a rough surface finish. Zhang et al. [14] investigated the effect of the lubricating method on the surface quality between the Mg alloy sheet

and tool in warm SPIF and found an association of the adhesive wear to temperature and lubrication method. Göttmann et al. [15] found that the strong abrasive wear of the tools and the worked metal sheet surfaces of titanium is a typical problem in the warm SPIF.

Surface quality is an important standard to determine product quality. More complicated factors affect the surface quality of SPIF parts than that of conventional sheets forming. Several scholars have examined the effect of various process parameters, such as feed rate, forming force, step size, tool diameter, tool shape, spindle speed, wall angle, and lubrication conditions on the surface roughness of different parts formed by SPIF. Mulay et al. [16] investigated the influence of the step depth, feed rate, and tool radius on the surface roughness of the formed parts. Ajay and Vishal [17], in their study of the influence of different tool shapes on surface roughness, highlighted that the surface quality of parts formed with hemispherical tool shape is better than other parts. Wang et al. [18] argued that a reasonable combination of the rotating speed of the tool and step depth could improve surface quality. Attanasio et al. [19] observed the best surface quality on an automotive component with the optimization of the tool path in two-point sheets incremental forming. Diabb et al. [20] and Xu et al. [21] observed an improvement in the surface quality of Mg alloy by changing the lubricating methods on the sheet in warm SPIF. Zhang et al. [14] improved the surface quality of Mg alloy in warm SPIF using a novel lubricating method in which the potassium titanium oxide ($K_2Ti_4O_9$) whisker was used.

In other respects, Sisodia and Kumar [22] used a dummy sheet to avoid the direct contact between tool and target sheet and revealed that the existence of a dummy sheet significantly improved the final surface quality of the target sheet. Amini et al. [23] studied the SPIF process of AA 1050 aluminum sheets using ultrasonic vibration (UV) numerically and experimentally. The results showed that applying UV would increase sheet formability and decrease surface roughness. Long et al. [24] and Li et al. [25] studied the impact of ultrasonic vibration on force reduction and deformation behavior of Al alloy in SPIF at room temperature. They documented that the UV could decrease forming force and friction. Sakhtemanian et al. [26] investigated the effect of UV-assisted on the SPIF process of St/Ti bimetal sheet at room temperature and showed that ultrasonic vibration decreased the coefficient of friction and refined grains. The effectiveness of ultrasonic vibrations to improve the surface quality also occurs in other forming processes such as grinding [27], polishing [28], bending [29], and grinding [30], etc. The impacts of UV on the surface quality of the SPIF process in hot conditions, however, remain undefined.

In the current study, ultrasonic vibration was introduced into the warm SPIF process of Mg alloy. The roughness and surface topography of Mg alloy surfaces were measured. The effects of the ultrasonic vibration on surface quality, including orange peel and adhesive wear, were examined. The intrinsic relation between the orange peel and microstructure of Mg alloy is explored with the use of microstructure examination. Lastly, the effect of three kinds of lubricants on contact surface quality was analyzed.

# 2. Experiment Details

The experiments were conducted on a 3-axis Computer Numerical Control (CNC) milling machine, as shown in Fig. 1 (a). A heat insulation platform, composed of a blank holder and support plate, was built on the machine to support the Mg alloy sheet. A hot air heating system was established to heat the sheet. The air was heated when it flew through the heating coils, and then flew into the heat insulation platform. An infrared camera was employed to monitor the temperature distribution on the deforming Mg alloy sheet. An infrared temperature sensor was used to collect the temperature signals. It could feed the signals back to the PID control system to adjust the power of the heating system (see Ref. [8] for complete details). A UV device, which can convert high-frequency electrical signals to vibration signals, was designed and integrated into the spindle of the CNC machine, as shown in Figs. 1 (b) and (c). It primarily consists of a generator, a transducer, an amplitude amplifier, and a hemispherical forming tool (made of cemented carbide). The transducer receives the high-frequency current signals generated by the ultrasonic generator through the connector. Then the electrical energy is converted to mechanical vibration by the transducer through inverse piezoelectric effects. The created vibration is amplified by the amplitude amplifier and transmitted to the forming tool. The vibration is noticed along the forming tool axial direction (Z-direction), which shows a periodic discontinuous contact state with sheets. A cooling system is applied to make the transducer work at a relatively low temperature.

A series of experiments at different temperatures (200 ℃, 225 ℃, 250 ℃, and 275 ℃) and ultrasonic amplitudes (0 μm, 3.8 μm, 7.8 μm, and 11.2 μm) were conducted to study the effects of UV on surface quality in warm SPIF process. The AZ31B Mg alloy sheet was used as the experimental material. And the target forming part was a square pyramid, as shown in Fig. 2. Based on the contour line path of the square pyramid, a G-code program was written by UG and sent to the CNC apparatus. The graphite grease was utilized to lubricate the interface between tool and sheet and was painted evenly on the surface of the Mg alloy sheet. Table 1 summarizes the process parameters of UV-assisted warm SPIF.

Table 1
The process parameters of UV-assisted warm SPIF

| Size of sheet | Thickness of sheet | Feed rate | Tool diameter | Angle of forming | Depth of forming | Step size |
|---|---|---|---|---|---|---|
| 200×200 mm | 1 mm | 1000 mm/min | 10 mm | 40° | 35 mm | 0.35 mm |

The quantitative 3D surface topography (and roughness profile) measurements were conducted using a white light interferometer (STIL, MICROMESURE 2), while the surface topography of each specimen was observed by an optical microscope. One of the side walls was selected as a representative of each formed part, as shown in Fig. 2. Five different areas are evenly selected on the sidewall, including the contact surface (contact with the tool) and the non-contact surface. Then an average roughness of the five areas in each wall was defined as the final value. The size of the sampling area was 3 × 3 mm; a sampling interval of 10 μm at a scanning speed of 1 mm/s was selected. A Gauss filter with a cut-off frequency of 0.015 was used to separate the roughness components and noise.

# 3. Results And Discussion

# 3.1 Orange peel patterns on the non-contact surface

## 3.1.1 Macro analysis

A rough texture, which resembles the shape of an orange peel, is generated on the non-contact surface of the Mg alloy during the warm-assisted SPIF (Fig. 3(a)). Figure 3 shows the distinct directionality of the orange peel. They are generated along with the transverse directions (TD) of the sidewall. The morphology, size, and density of the orange peel patterns are significantly influenced by the forming temperatures and ultrasonic amplitudes. Figure 3(a-d) shows a comparison of the texture of orange peel morphology of the sidewall at different temperatures. At 200°C temperature, the texture of orange peel is coarse and unevenly distributed with small pits. Furthermore, local microcracks and local necking phenomena [11] can be observed on the surface of the parts. When the forming temperature increases to 250°C, the texture of the orange peel gets thinner and shallower. But it turns coarse with shallow pits again at 275°C. Figures 3(a, e, f, g) show the effect of UV on the orange peel morphology of the sidewall at 200°C. With an increase in amplitude, the texture of the orange peel of the formed part becomes finer, lighter, and more even. No microcracks and local necking phenomenon can be seen. The same situation is seen at other temperatures. Although at 250°C and 275°C, the orange peel patterns tend to turn coarser again at the amplitude of 11.2 μm.

## 3.1.2 Roughness analysis

Figure 4 depicts the evolution of roughness of the non-contact surface of formed parts at different temperatures and ultrasonic amplitudes. The roughness of the original sheet is 3.6 μm, but after the forming, the average roughness of all formed parts is over 5 μm. The significant increase in roughness is primarily due to the appearance of orange peel texture. The roughness of the orange peel declines as the temperature increases from 200°C to 250°C and is decreased by approximately 11.9%. However, it starts increasing when the forming temperature reaches 275°C. UV can effectively reduce the roughness of the formed parts at all temperatures. When the amplitude is increased from 0 μm to 11.2 μm, roughness (Ra) is decreased by a maximum of 20.2%, 7.3%, 14.2% and 11.7% for 200°C, 225°C, 250°C, and 275°C temperature, respectively. The applied ultrasonic vibration has the most significant effect on orange peel roughness at 200°C. While at the temperature of 250°C and 275°C, the excessive amplitude can cause the roughness values to increase again.

## 3.1.3 3D topography analysis

Figure 5 shows the 3D topography plots of orange peel patterns on the non-contact surface. The altitude distribution of orange peels on each surface is measured in the same base level. Figures 5(a-d) show that higher fluctuations of the surface height between orange peel patterns are observed at 200°C. And typical concave pits in irregular distribution are fabricated. The orange peels are bumpy and undulating to the

maximum extent, resulting in the highest roughness. As the temperature increases, shallower orange peel patterns are observed at 250°C. But the patterns turn coarse again at 275°C. As per Fig. 5(a, e, f, g), with the increase of ultrasonic amplitude at 200°C, the orange peel patterns become lighter, flatter, and evenly distributed. Compared with that at 250°C, the area of protruding orange peels (red area in Fig. 5) is reduced more significantly after applying appropriate UV at 200°C. Figure 5(c, h, i, j) shows that the flatter orange peel patterns can be further improved after applying the UV at 250°C temperature. But it turns coarse again at high amplitude (11.2 μm). The situation is similar at the temperature of 275°C.

The above results show that both the ultrasonic vibration and proper temperature are advantageous in reducing the orange peel in warm SPIF of Mg alloys, thereby improving the non-contact surface quality. And the surface quality of orange peel can be improved remarkably by applying UV at the proper temperature.

# 3.1.4 Microstructure analysis

In order to further understand the effect of temperature and ultrasonic amplitudes on the orange peel, the microstructure of formed parts was analyzed after the UV-assisted warm SPIF process. The specimens of 10 × 10 mm dimension were cut at position 2 from the sidewall of the square pyramid-shaped specimens (Fig. 2). Figure 6 shows the microstructure of specimens at different temperatures and amplitudes. Fine dynamic recrystallization (DRX) grains [31], newly formed around the coarse grains, can be seen in SPIF specimens. They confirmed the occurrence of DRX during the deformation. Figure 6(a-d) depicts that the grain structure of the sample is highly unevenly distributed at 200°C. It tends to be homogeneous with the increase in the forming temperature. Moreover, the grains grow rapidly as the temperature rises. At 275°C, many oversized grains can be found. Figure 6(c, e, f, g) indicates that with an increase in the amplitude (from 0 to 7.8 μm) at 250°C, the number of fine grains increases sharply. It indicates that UV can promote DRX fully and refine grains during the forming process. However, the fine grains have grown up when the amplitude reaches 11.2 μm. The excessive amplitude of UV coarsens the grains. The situation resembled other temperatures.

Figure 7 shows the average grain size of the specimens at different temperatures and ultrasonic amplitudes. The average grain size increases with rising temperature without UV-assisted process. The average grain sizes are 13 μm, 15 μm, 23.5 μm, 36 μm at the temperature of 200°C, 225°C, 250°C, 275°C, respectively. A few grains achieve the maximum size of 60 □ 70 μm at 275°C. After applying the UV, the average grain size decreases significantly with the promotion of DRX. As the ultrasonic amplitude reaches 7.8 μm, the average grain size of grains at each temperature decreases to 9.6 μm, 11 μm, 15.5 μm, 19 μm, respectively due to better DRX. When amplitude reaches 11.2 μm, the fine grains begin to grow, increasing the average grain size.

At 200°C temperature without UV-assisted, unevenly distributed grain structure can be observed in Fig. 6a and the oversized grains can be observed at 275°C (Fig. 6d). The previous sections show more pronounced orange peel patterns under these forming conditions. Hence, the occurrence of orange peel

patterns is related to the unevenly distributed grain structure and the oversized grains of the sheet in the warm SPIF process. These findings corroborate those in previous studies [8, 9].

# 3.2 Contact surface quality

Figure 8 illustrates the schematic diagram of the tool-sheet contact for SPIF. The surface quality of the Mg alloy of the contact surface during the warm SPIF is primarily affected by three parts. First, the residual wave (Fig. 12(c)) can be observed in region A. It is related to tool diameter, step size, and forming angle. Second, the adhesive wear and scratches, etc. (Fig. 10(c)) can be observed chiefly in region B. They are related to the temperatures and lubrication conditions. Finally, the transverse vein (Fig. 10(a)) generated along the movement direction can be observed in region C.

## 3.2.1 Roughness analysis

Figure 9 shows the roughness (Ra) evolution of the contact surface of the formed parts at different temperatures and ultrasonic amplitudes. After the warm SPIF process, the roughness values of the contact surface of all formed parts are over the original sheet. The increase in roughness is mainly due to the appearance of the several defects described in Fig. 8. According to Fig. 9, the roughness of the contact surface of the formed parts increases by approximately 7.6% as the temperature rises from 200°C to 250°C. But it tends to decrease when the forming temperature reaches 275°C. After UV is applied, the roughness of the formed parts at all temperatures is effectively decreased. When the amplitude is increased from 0 μm to 7.8 μm, Ra reduces by approximately 11.1%, 15.6%, 29.6%, and 26.3% for 200°C, 225°C, 250°C, and 275°C temperature, respectively. Ultrasonic vibration has the most significant effect on contact surface roughness at 250°C. At 11.2 μm amplitude, Ra begins to increase. Appropriate UV has positive effects on reducing the roughness of contact surfaces, resulting in better surface quality.

## 3.2.2 The 3D topography and Surface topography analysis

The 3D topography and surface topography of the contact surface of formed parts at different temperatures are illustrated in Fig. 10($a_2$-$d_2$, $a_3$-$d_3$). Figure 10 ($a_1$-$d_1$) shows the 2D profile texture curves measured along the rolling direction (RD). Surface defects such as residual wave, scratches, adhesion, pits, and the transverse vein, etc. are observed in the inner surface of the parts, as shown in Fig. 10. When the temperature increases from 200°C to 250°C, increasingly conspicuous scratches are observed on the residual wave and transverse vein of the contact surface. They appear as sharp waviness in the 2D profile curve. The depth and number of scratches increase with the rising temperature; then the surface finish gets worse. In addition, some pits and adhesion are observed at 250°C, which shows exacerbated oxidation and adhesive wear. Under high temperature and high contact pressure conditions, a lot of wear debris is peeled off while pits are formed during the warm SPIF process. The wear debris sticks on the tool and forms scratch at the tool-sheet interface, resulting in a rough surface finish [15]. When the temperature reaches 275°C, obvious adhesive wear is observed on the surface with scarce scratches, as illustrated in Fig. 10 ($d_2$, $d_3$). The failure of grease and softening of material at 275°C are the key reasons

that tend to increase the adhesive wear [32]. One of the reasons for the reduction of surface scratches may be the plastic deformation of small debris within the surface layers of alloy [33]. Adhesive wear can promote the flow of material on the contact surface, which will cover the scratches.

In order to analyze the mechanism of an ultrasonic vibration for the reduction of contact surface roughness after the warm SPIF process, the textures of the residual wave at 250°C are analyzed. It is measured along the vertical feed direction (Fig. 12($b_1$)). Figure 11 shows that periodic waviness peaks represent residual waves generated by SPIF in the 2D texture curve. The sharp peaks and valleys on the residual wave represent the scratches. As the amplitude increases to 7.8 μm, the residual waves get more rounded and the residual height (Fig. 8) values become lower. The reciprocating motion generated by the UV tool flattens residual wave height on the rippling surface. It also reduces the scratches, smoothening the surface. But when the amplitude reaches 11.2 μm, the residual wave height tends to increase, and the roughness value increases. The reasons are analyzed in the next section.

Thereafter, the 3D topography and surface topography of the contact surface at 250°C are analyzed, as shown in Fig. 12. As the UV amplitude increases to 7.8 μm, the number and depth of scratches show an obvious decrease; the pits and adhesive wear are significantly decreased. A relatively flat and smooth residual wave surface with the lowest surface height fluctuations is noticed at 7.8 μm (Fig. 12(c)). In conventional warm SPIF, the grease between the tool-sheet interfaces is easily squeezed out, and dry friction occurs. The reciprocating motion of the ultrasonic tool head can prevent this and improve the lubrication effect. It can reduce the shear stress of friction pairs [26], then reducing pits and adhesion. Furthermore, it can restrict the origination and propagation of debris scratches. But when the amplitude reaches 11.2 μm, the accumulation of material next to the transverse vein can be found due to the excessive vibration. Further, it deepens the transverse vein (Fig. 12(d)). This accounts for an increase in roughness and residual wave height, as aforementioned. The situation is similar at other temperatures also.

# 3.3 The effect of lubricants on surface quality

In this study, three types of lubricants were investigated in warm SPIF with or without ultrasonic-assisted at 250°C, as shown in Table 2. The surface roughness Ra, 3D topography, and surface topography were used to assess the surface quality of different formed parts. When UV is not applied, the surface roughness is 5.9 μm, 6.2 μm, and 7.6 μm under the molybdenum disulfide ($MoS_2$) powder, graphite grease, and $MoS_2$ grease lubrication conditions, respectively. At this condition, the bonding strength at the lubrication coating/sheet interface influences the lubrication effect [14]. Lubricant with strong bonding strength cannot be completely squeezed out from the surface of the sheet during SPIF, thereby improving the lubrication effect. Table 2 shows that the bonding strength with a sheet of $MoS_2$ grease is stronger than others at 250°C, suggesting a better lubrication effect of $MoS_2$ grease. However, the corresponding roughness value of $MoS_2$ grease is maximum due to some reasons. After applying UV with an amplitude of 7.8 μm, the roughness is reduced by approximately 26.9%, 29.6%, and 30.4%, respectively. At this

amplitude, the bonding strength of the lubrication coating/sheet interface is no longer the main factor affecting the surface quality.

Table 2
Types of different lubricants used in warm SPIF

| Lubricants | Models and Brands | Bonding strength at 250°C | Application method | Ra (A = 0 μm) | Ra (A = 7.8 μm) |
|---|---|---|---|---|---|
| $MoS_2$ powder | $FMoS_2$-2, Efficient | Weak | Painted with acetone | 5.9 μm | 4.31 μm |
| Graphite grease | GX-501, YAMATE | Medium | Painted | 6.2 μm | 4.37 μm |
| $MoS_2$ grease | Futu lube | Strong | Painted | 7.6 μm | 5.29 μm |

### 3.3.1 The 3D topography and surface topography analysis

The 3D topography and surface topography of contact surface in warm SPIF with or without ultrasonic under different lubrication are shown in Figs. 13 and 14. Under $MoS_2$ powder lubrication, the lubricant is entirely squeezed out from the surface of the sheet in SPIF. Adhesive wear is observed, and dry friction is predominant [14, 32], significantly damaging the surface of the tool and formed parts. Under graphite grease lubrication, scratches and local adhesive wear are observed. UV application can appreciably decrease the adhesive wear and scratches generated in $MoS_2$ powder and graphite grease lubrication, as shown in Fig. 14(e, f). The reasons for this have been examined in the previous section. While under $MoS_2$ grease lubrication, many deep cracks along the RD and flaking pits can be found due to oxidation wear [34] without adhesive wear, as shown in Fig. 14(c). Since $MoS_2$ grease has remarkable bonding strength with the sheet, the direct contact between the tool and the sheet is slightly avoided, thus reducing adhesive and abrasive wear. Compared with the surface topography with other lubrication conditions (Fig. 14), $MoS_2$ grease seems to aggravate the oxidation behavior of the Mg alloy surface at high temperatures. And it exacerbates the generation of cracks and flaking pits in warm SPIF under a high contact pressure condition, thereby worsening surface finish. But the UV can decrease the contact pressure [24], which can restrict the origination and propagation of deep cracks and flaking pits, as shown in Fig. 14(g).

Indeed, the lubricant with strong bonding at the lubrication coating/sheet interface can effectively reduce the adhesive wear of the contact surface and improve lubricating effects. But it also needs to consider other problems, such as cracks in $MoS_2$ grease and wear on the tool in $MoS_2$ powder caused by lubricants. Considering all these factors, graphite grease is more suitable for use in the warm SPIF among the three lubricants.

## 4. Conclusions

In the current study, UV-assisted warm SPIF experiments of AZ31B are performed. The orange peel patterns on the non-contact surface at different temperatures and ultrasonic amplitudes were examined, along with the scratches and adhesion phenomenon on the contact surface. Microstructure examinations were conducted to evaluate the influence of heating and UV parameters on the orange peel patterns. The effect of different lubricants on surface quality is also studied. The following main conclusions can be drawn:

(1) A greater forming temperature helps to reduce the orange peel patterns in the non-contact surface of the parts. However, a further increase of the forming temperature results in coarse grains, leading to rougher orange peel patterns. The application of UV can promote the DRX of Mg alloy during the warm SPIF to refine the grains, which is useful in reducing the orange peel patterns.

(2) As the temperature increases, obvious abrasive and adhesive wear can be found on the contact surfaces of the formed parts in the warm SPIF. The application of UV can reduce the contact and friction between friction pairs, thereby reducing the scratches and adhesion phenomenon effectively at high temperatures.

(3) Among the tested values, the forming temperature of 250°C with an amplitude of 7.8 μm gives the best surface quality of both surfaces. The excessive vibration amplitude (11.2 μm) deepens the transverse vein on the contact surface and generates material accumulation next to the transverse vein, increasing the roughness value.

(4) Following conditions are required for the choice of lubricant for SPIF at a high temperature: high-temperature resistance, strong bonding at the lubrication coating/sheet interface, and the ability to prevent the oxidation behavior of Mg alloy surface in high temperature.

To sum up, the application of UV can improve surface quality under various lubrication conditions. Besides reducing scratches and adhesive wear, it can restrict the origination and propagation of deep cracks and flaking pits produced due to high contact pressure and oxidation wear of warm SPIF.

# Declarations

**Acknowledgements** The authors would like to express many thanks to Mr. Jianhua Liu for the help of some experimental work and suggestions.

**Authors' contributions** All authors contributed equally to the generation and analysis of experimental data, and the development of the manuscript.

**Funding** This work received the financial support by the National Natural Science Foundation of China (No. 51805087).

**Code availability** Not applicable

**Availability of data and material** This study is based only on data obtained using the methods described in this paper

**Ethics approval** All authors declare that his article does not have any academic ethics issues and strictly follows the journal submission rules.

**Consent to participate** All authors agree to participated in this research work.

**Consent for publication** All authors agree to publish this work.

**Conflict of interest** The authors declare no competing interests.

# References


1. Kojima Y, Kamado S (2005) Fundamental Magnesium Researches in Japan. Mater Sci Forum 518:9–16
2. Kawalla R, Ullmann M, Henseler T, Prahl U (2019) Magnesium Twin-Roll Casting Technology for Flat and Long Products-State of the Art and Future. Mater Sci Forum 45591431–1436
3. Palumbo G, Sorgente D, Tricarico L (2008) The design of a formability test in warm conditions for an AZ31 magnesium alloy avoiding friction and strain rate effects. Int J Mach Tool Manuf 48:1535–1545
4. Zhang KF, Yin DL, Wu DZ (2006) Formability of AZ31 Magnesium Alloy Sheets at Warm Working Conditions, Int J Mach Tool Manuf. 461276–1280
5. Campanella D, Buffa G, Valvo EL, Fratini L (2021) A numerical approach for the modelling of forming limits in hot incremental forming of AZ31 magnesium alloy. Int J Adv Manuf Technol (prepublish)
6. Su CJ, Zhao ZX, Lv YT, Wang R, Wang Q, Wang MY (2019) Effect of Process Parameters on Plastic Formability and Microstructures of Magnesium Alloy in Single Point Incremental Forming. J Mater Eng Perform 28:7737–7755
7. Leonhardt A, Kurz G, Victoria-Hernández J, Kräusel V, Landgrebe D, Letzig D (2018) Experimental study on incremental sheet forming of magnesium alloy AZ31 with hot air heating. Procedia Manuf 15:1192–1199
8. Liao J, Liu JH, Zhang LX, Xue X (2020) Influence of heating mode on orange peel patterns in warm incremental forming of magnesium alloy. Procedia Manuf 5:5–10
9. Davis JR (1992) ASM Materials Engineering Dictionary. ASM Int, Geauga, p 298
10. Carter JT, Krajewski PE, Verma R (2008) The hot blow forming of AZ31 Mg sheet: Formability assessment and application development. JOM 60:77–81
11. Antoniswamy AR, Carpenter AJ, Carter JT, Hector LG, Tale-Ff EM (2013) The Influence of Deformation Mechanisms on Rupture of AZ31B Magnesium Alloy Sheet at Elevated Temperatures. Magnesium Technol 34:211–215

12. Duflou JR, Callebaut B, Verbert J, De Baerdemaeker H (2007) Improved SPIF performance through dynamic local heating. Int J Mach Tool Manuf 48:543–549
13. Xu DK, Lu B, Cao TT, Zhang H, Chen J, Long H, Cao J (2016) Enhancement of process capabilities in electrically-assisted double sided incremental forming. Mater Design 92:268–280
14. Zhang QL, Xiao FG, Guo HL, Li CS, Gao L, Guo XW, Han WD, Bondarev AB (2009) Warm negative incremental forming of magnesium alloy AZ31 Sheet: New lubricating method. J Mater Process Tech 210:323–329
15. Göttmann A, Diettrich J, Bergweiler G, Bambach M, Hirt G, Loosen P, Poprawe R (2011) Laser-assisted asymmetric incremental sheet forming of titanium sheet metal parts. Production Eng 5:263–271
16. Mulay A, Ben S, Ismail S, Kocanda A (2017) Experimental investigations into the effects of SPIF forming conditions on surface roughness and formability by design of experiments. J Braz Soc Mech Sci 39:3997–4010
17. Ajay K, Vishal G (2018) Experimental investigation and optimization of surface roughness in negative incremental forming. Measurement 131:419–430
18. Wang ZH, Cai S, Chen J (2020) Experimental investigations on friction stir assisted single point incremental forming of low-ductility aluminum alloy sheet for higher formability with reasonable surface quality. J Mater Process Tech 277:116488
19. Attanasio A, Ceretti E, Giardini C (2006) Optimization of tool path in two points incremental forming. J Mater Process Tech 177:409–412
20. Diabb J, Rodríguez CA, Mamidi N, Sandoval JA, Taha-Tijerina J, Martínez-Romero O, Elías-Zúñiga A (2017) Study of lubrication and wear in single point incremental sheet forming (SPIF) process using vegetable oil nanolubricants. Wear 376–377:777–785
21. Xu CX, Li YL, Wang ZJ, Cheng ZN, Liu FY (2020) The influence of self-lubricating coating during incremental sheet forming of TA1 sheet. Int J Adv Manuf Technol 110:2465–2477
22. Sisodia V, Kumar S (2018) Influence of process parameters on surface roughness in single point incremental forming using dummy sheet. IOP Conf Ser: Mat Sci Eng 361
23. Amini S, Gollo AH, Paktinat H (2017) An investigation of conventional and ultrasonic-assisted incremental forming of annealed AA1050 sheet. Int J Adv Manuf Technol 90:1569–1578
24. Long YY, Li YL, Sun J, Ille I, Li JF, Twiefel J (2018) Effects of process parameters on force reduction and temperature variation during ultrasonic assisted incremental sheet forming process. Int J Adv Manuf Technol 97:13–24
25. Li Z, Wang, Li S, Li Z (2020) Investigation on the material flow and deformation behavior during ultrasonic-assisted incremental forming of straight grooves. J Mater Res Technol 9:433–454
26. Sakhtemanian MR, Honarpisheh M, Amini S (2019) A novel material modeling technique in the single-point incremental forming assisted by the ultrasonic vibration of low carbon steel/commercially pure titanium bimetal sheet. Int J Adv Manuf Technol 102:473–486

27. Tawakoli T, Azarhoushang B (2008) Influences of ultrasonic vibrations on dry grinding of soft steel. Int J Mach Tool Manuf 48:1585–1591
28. Zhao QL, Sun ZY, Guo B (2016) Material removal mechanism in ultrasonic vibration assisted polishing of micro cylindrical surface on SiC. Int J Mach Tool Manuf 103:28–39
29. Brehl DE, Dow TA (2007) Review of vibration-assisted machining. Precis Eng 2:153–172
30. Yin L, Zhao B, Huo BJ, Bie WB, Zhao CY (2021) Analytical modeling of grinding force and experimental study on ultrasonic-assisted forming grinding gear. Int J Adv Manuf Technol 114:3657–3673
31. Zhang HR, Chu XR, Lin SX, Bai HW, Sun J (2021) Temperature Influence on Formability and Microstructure of AZ31B during Electric Hot Temperature-Controlled Incremental Forming. Materials 14:810
32. Chang ZD, Chen J (2019) Analytical model and experimental validation of surface roughness for incremental sheet metal forming parts. Int J Mach Tool Manuf 146:103453
33. Kubo S, Kato K (1998) Effect of arc discharge on wear rate of Cu-impregnated carbon strip in unlubricated sliding against Cu trolley under electric current. Wear 21:172–178
34. Formisano A, Durante M, Boccarusso L, Astarita A (2017) The influence of thermal oxidation and tool-sheet contact conditions on the formability and the surface quality of incrementally formed grade 1 titanium thin sheets. Int J Adv Manuf Technol 93:3723–3732

# Figures

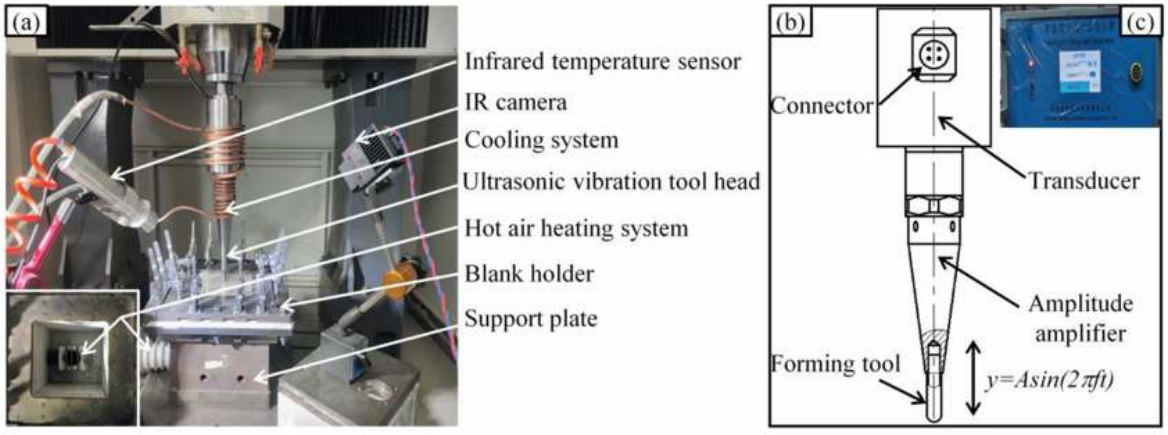


**Fig. 1** Equipment for UV-assisted warm SPIF: (a) Incremental forming platform; (b) Ultrasonic vibration tool head; (c) Ultrasonic generator.

**Figure 1**

See image above for figure legend.

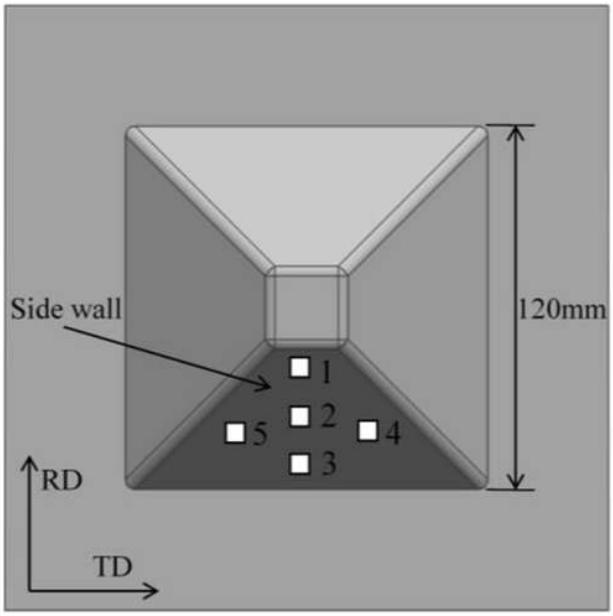


Fig. 2 Three-dimensional model of the square pyramid part.

## Figure 2

See image above for figure legend.

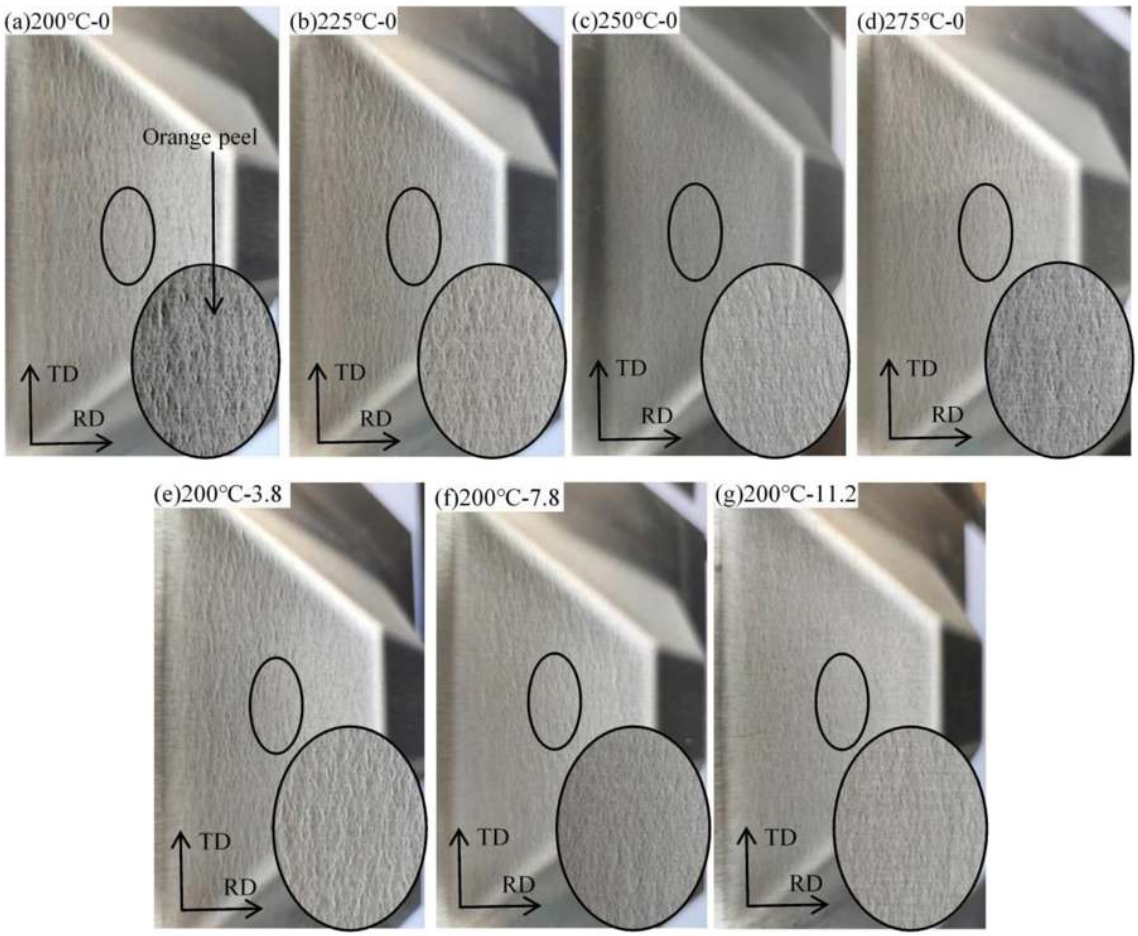


**Fig. 3** The deformed Mg alloy parts with orange peel patterns: (a) 200 °C-0 μm; (b) 225 °C-0 μm; (c) 250 °C-0 μm; (d) 275 °C-0 μm; (e) 200 °C-3.8 μm; (f) 200 °C-7.8 μm; (g) 200 °C-11.2 μm.

## Figure 3

See image above for figure legend.

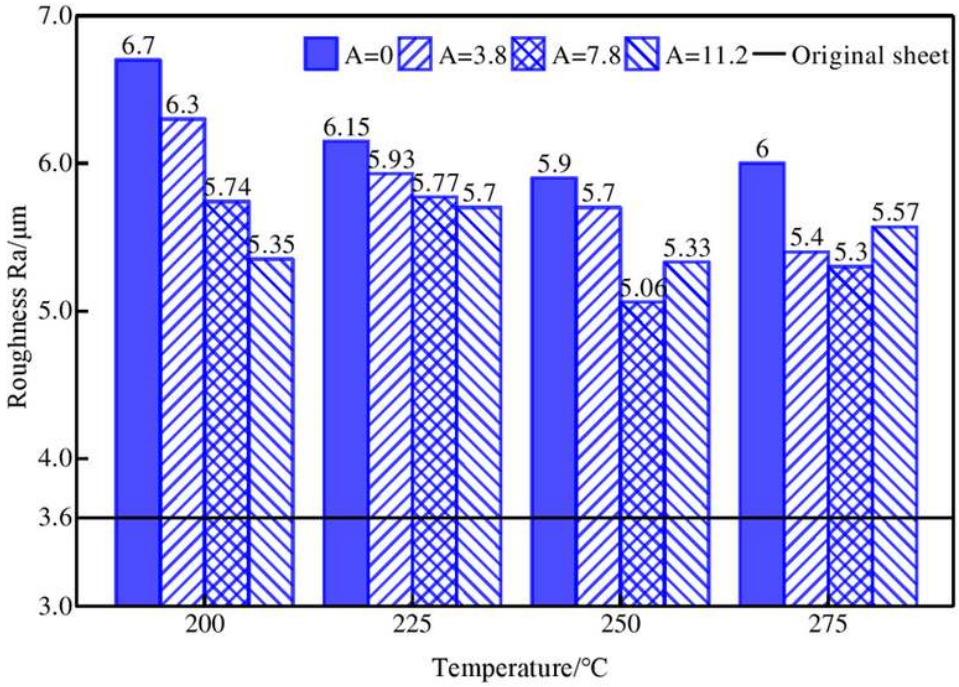


**Fig. 4** The evolution of roughness on the non-contact surface of formed parts.

## Figure 4

See image above for figure legend.

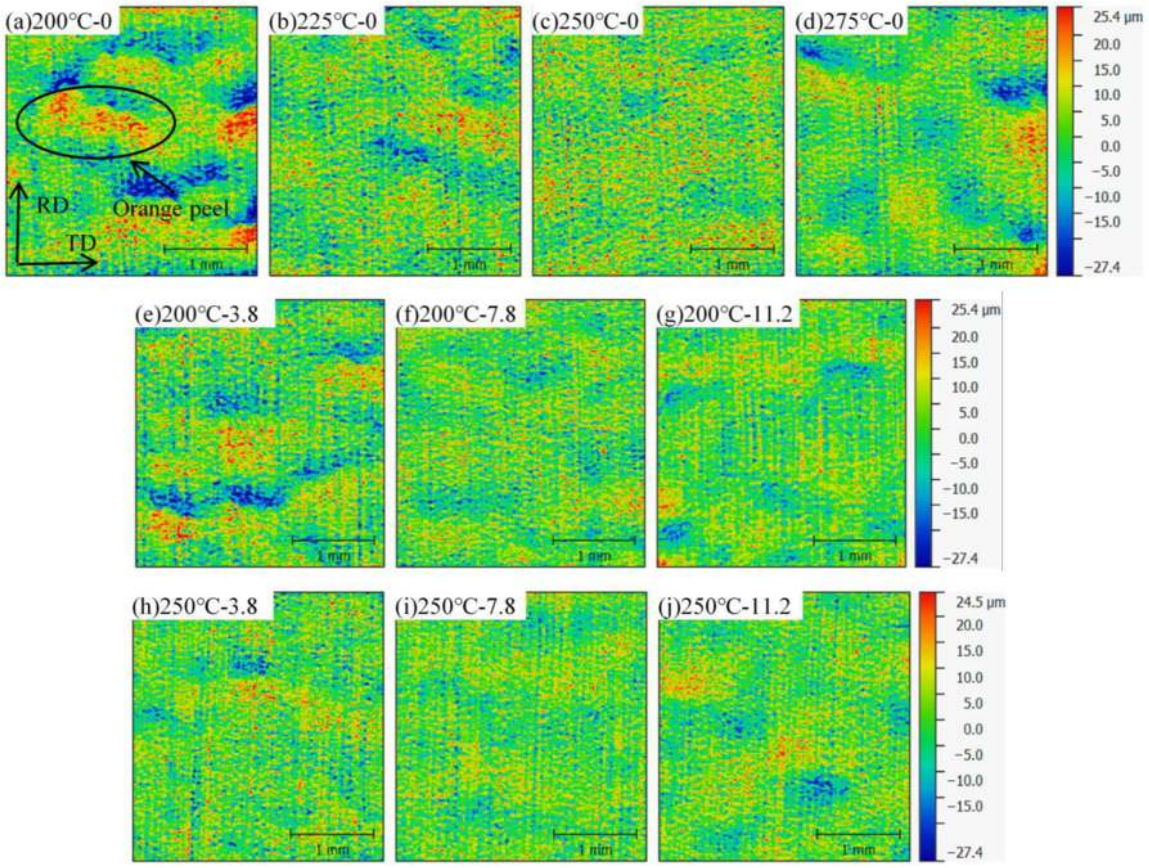


**Fig. 5** The 3D topography of orange peel on non-contact surface: (a) 200 °C-0 μm; (b) 225 °C-0 μm; (c) 250 °C-0 μm; (d) 275 °C-0 μm; (e) 200 °C-3.8 μm; (f) 200 °C-7.8 μm; (g) 200 °C-11.2 μm; (h) 250 °C-3.8 μm; (i) 250 °C-7.8 μm; (j) 250 °C-11.2 μm.

## Figure 5

See image above for figure legend.

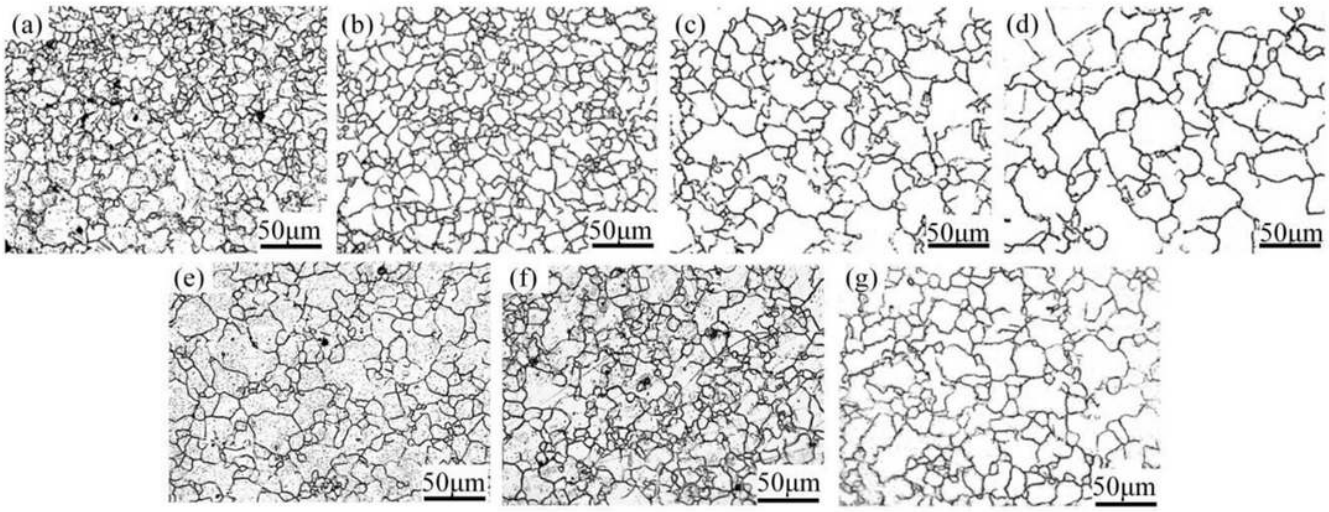


**Fig. 6** Microstructure of formed parts: (a) 200 °C-0 μm; (b) 225 °C-0 μm; (c) 250 °C-0 μm; (d) 275 °C-0 μm; (e) 250 °C-3.8 μm; (f) 250 °C-7.8 μm; (g) 250 °C-11.2 μm.

## Figure 6

See image above for figure legend.

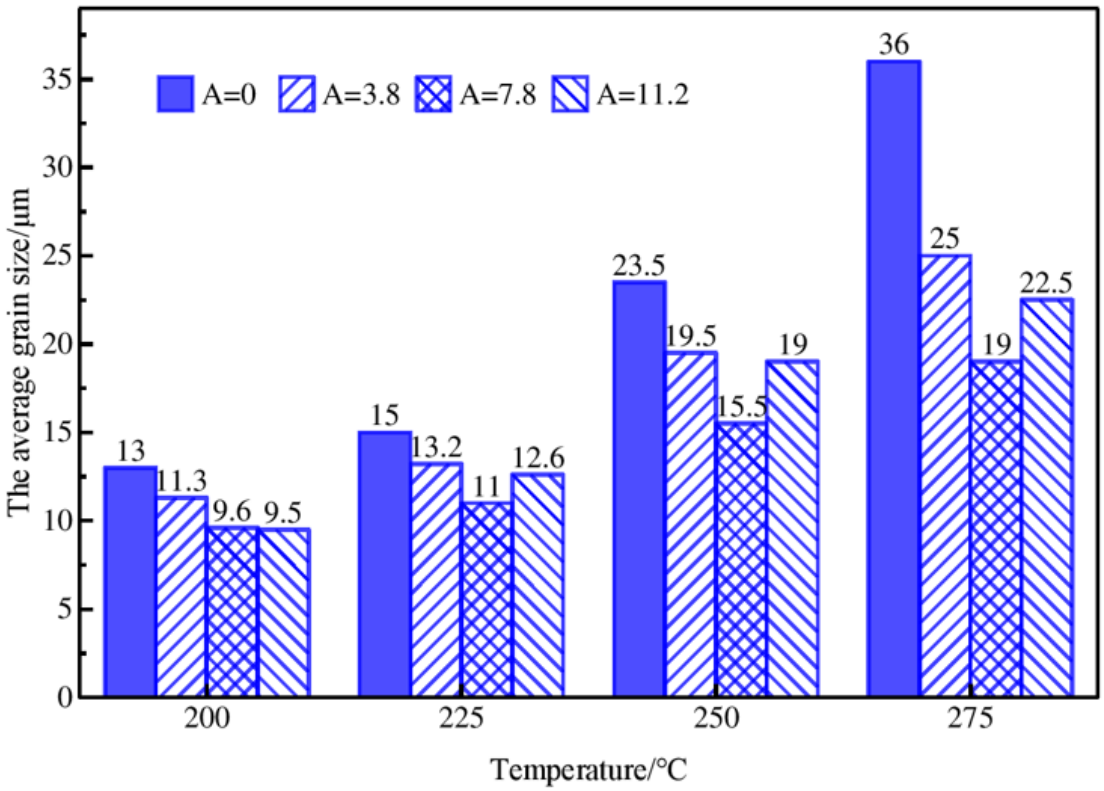


**Fig. 7** The average grain size of specimens after the SPIF process.

Figure 7

See image above for figure legend.

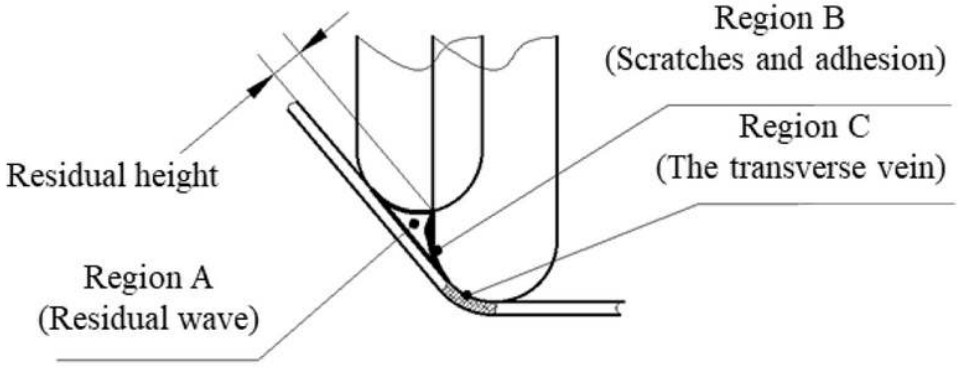


**Fig. 8** The schematic diagram of the tool-sheet contact for the SPIF process.

## Figure 8

See image above for figure legend.

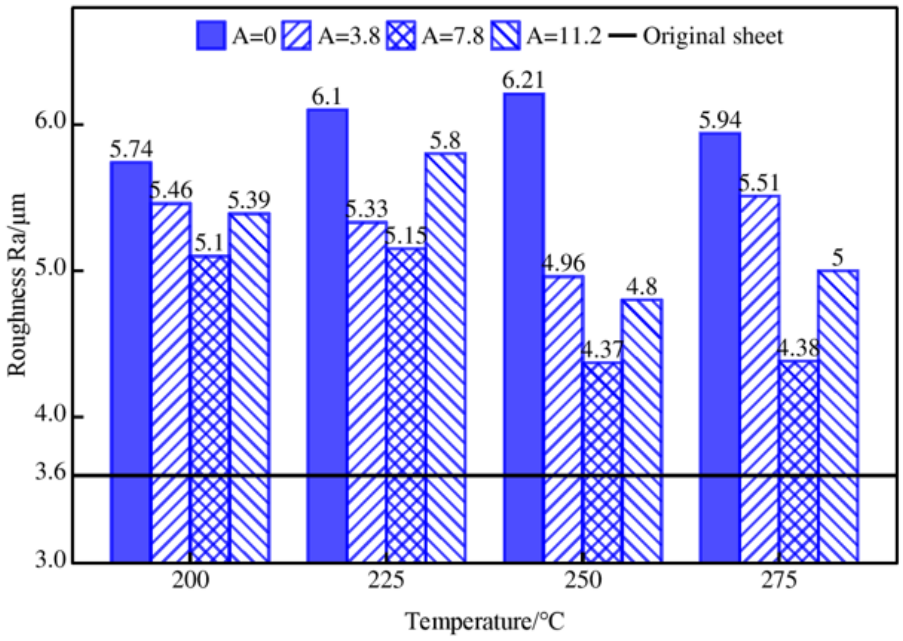


**Fig. 9** The evolution of roughness Ra on the contact surfaces of formed parts.

## Figure 9

See image above for figure legend.

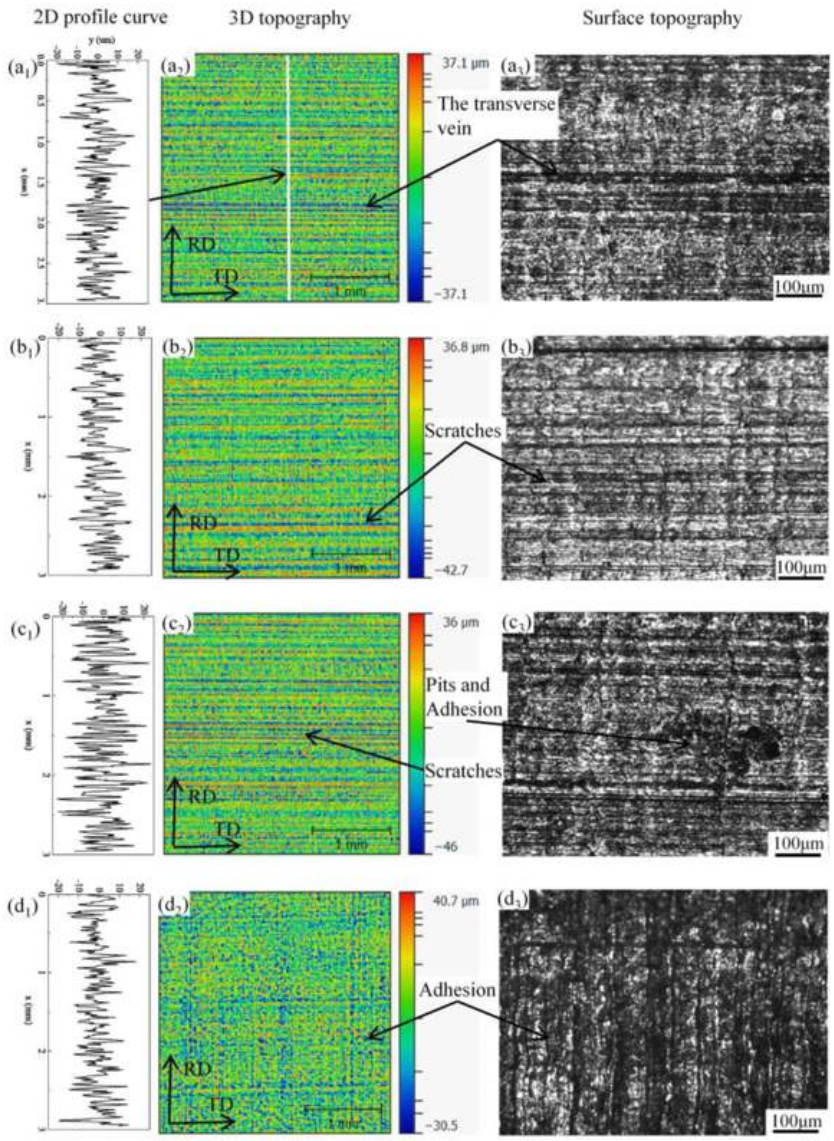


**Fig. 10** The 2D profile curve, 3D topography and surface topography of the sample: (a) 200 °C-0 μm; (b) 225 °C-0 μm; (c) 250 °C-0 μm; (d) 275 °C-0 μm.

## Figure 10

See image above for figure legend.

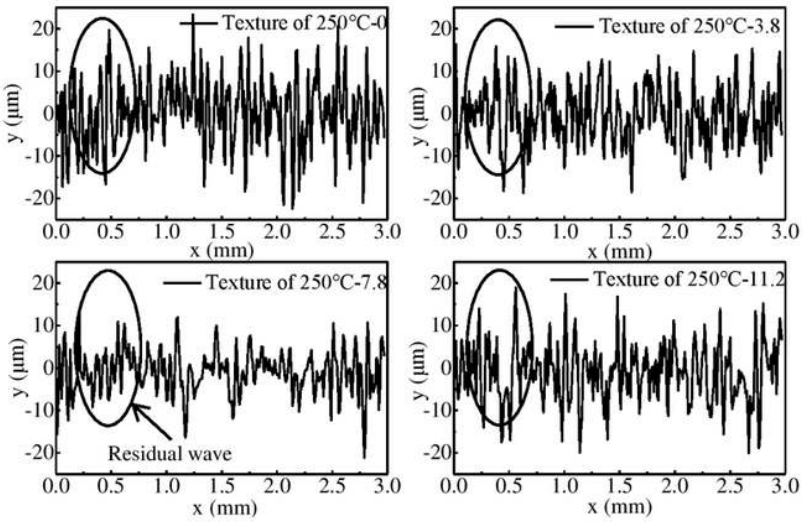


**Fig. 11** Comparison of residual wave on contact surface: (a) 250 °C-0 μm; (b) 250 °C-3.8 μm; (c) 250 °C-7.8 μm; (d) 250 °C-11.2 μm.

## Figure 11

See image above for figure legend.

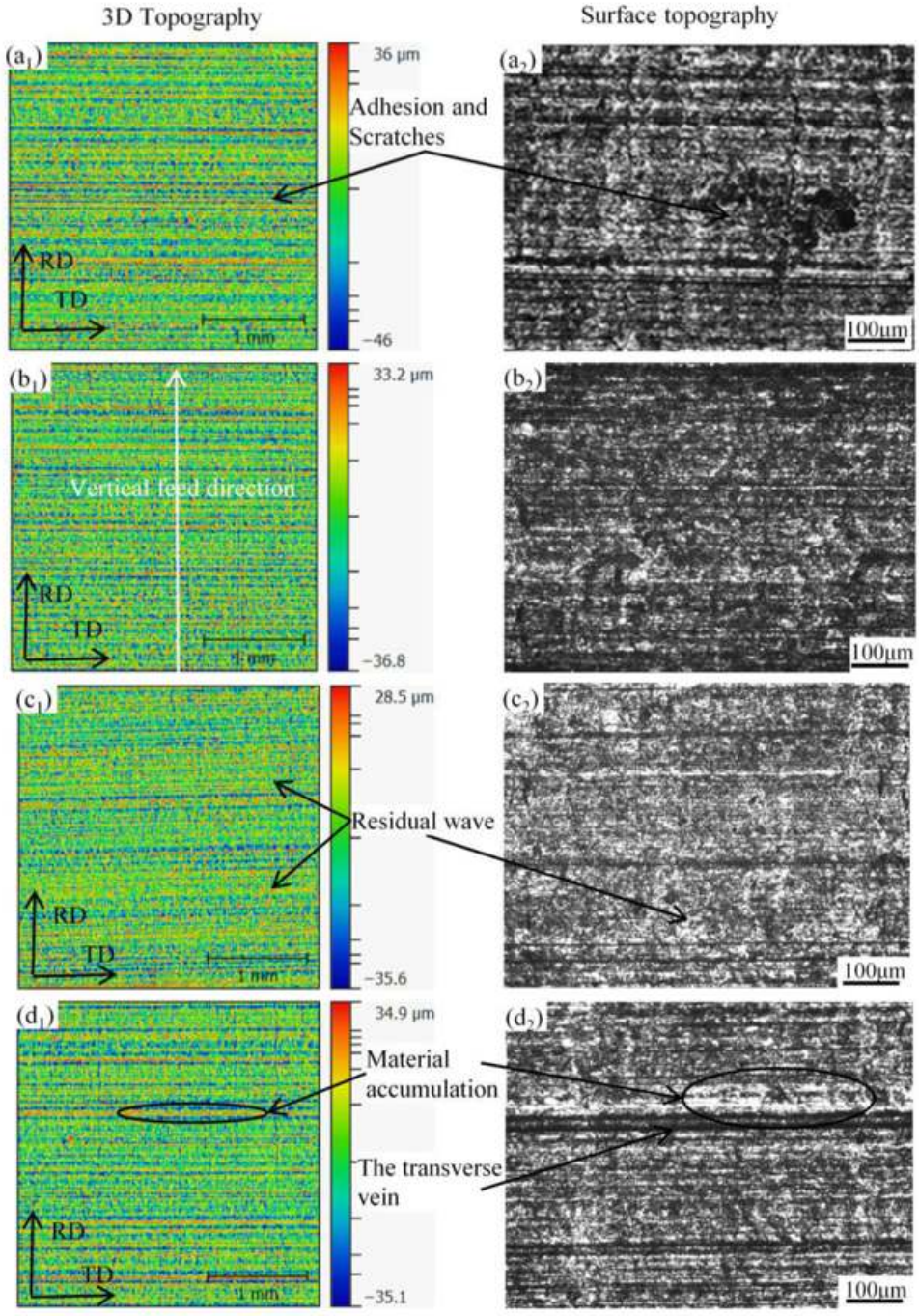


**Fig. 12** The 3D topography and the surface topography of the samples: (a) 250 °C-0 μm; (b) 250 °C-3.8 μm; (c) 250 °C-7.8 μm; (d) 250 °C-11.2 μm.

## Figure 12

See image above for figure legend.

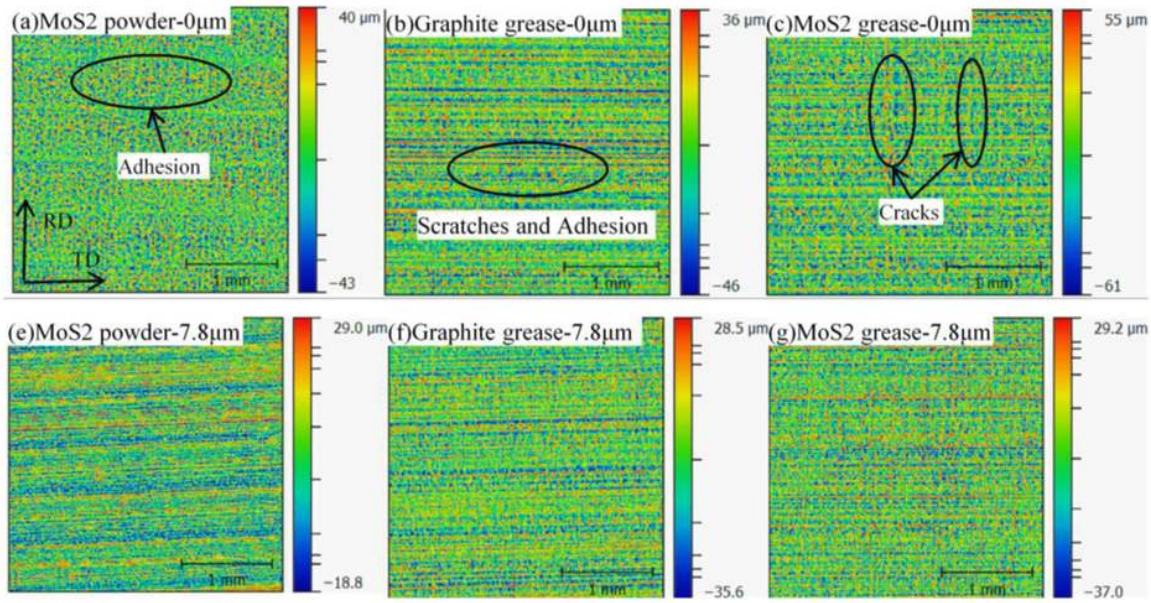


**Fig. 13** The 3D topography of the contact surface at 250 °C: (a) $MoS_2$ powder-0 μm; (b) Graphite grease-0 μm; (c) $MoS_2$ grease-0 μm; (e) $MoS_2$ powder-7.8 μm; (f) Graphite grease-7.8 μm; (g) $MoS_2$ grease-7.8 μm.

## Figure 13

See image above for figure legend.

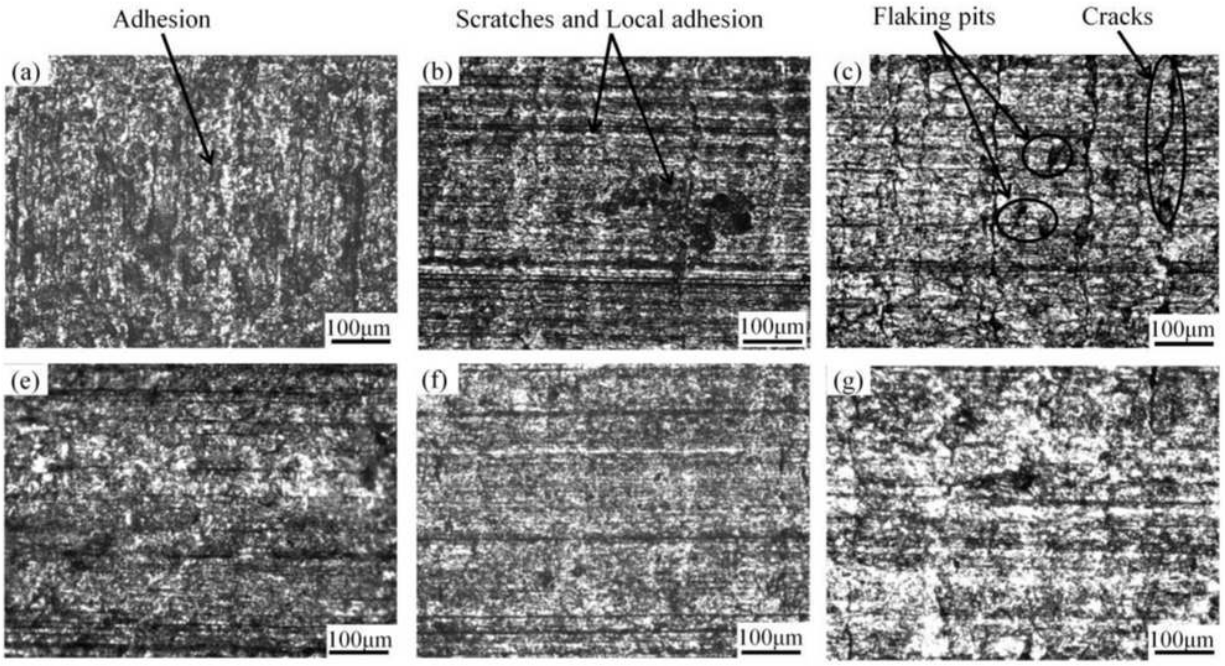


**Fig. 14** The surface topography of the contact surface at 250 °C: (a) $MoS_2$ powder-0 μm; (b) Graphite grease-0 μm; (c) $MoS_2$ grease-0 μm; (e) $MoS_2$ powder-7.8 μm; (f) Graphite grease-7.8 μm; (g) $MoS_2$ grease-7.8 μm.

## Figure 14

See image above for figure legend.